ARTICLES
https://doi.org/10.1038/s41565-022-01145-w
nature nanotechnology

Continuous cuffless monitoring of arterial blood pressure via graphene bioimpedance tattoos

Dmitry Kireev[1,2,6], Kaan Sel[3,6], Bassem Ibrahim[3], Neelotpala Kumar[1], Ali Akbari[4], Roozbeh Jafari[3,4,5] ✉ and Deji Akinwande[1,2] ✉

Continuous monitoring of arterial blood pressure (BP) in non-clinical (ambulatory) settings is essential for understanding numerous health conditions, including cardiovascular diseases. Besides their importance in medical diagnosis, ambulatory BP monitoring platforms can advance disease correlation with individual behaviour, daily habits and lifestyle, potentially enabling analysis of root causes, prognosis and disease prevention. Although conventional ambulatory BP devices exist, they are uncomfortable, bulky and intrusive. Here we introduce a wearable continuous BP monitoring platform that is based on electrical bioimpedance and leverages atomically thin, self-adhesive, lightweight and unobtrusive graphene electronic tattoos as human bioelectronic interfaces. The graphene electronic tattoos are used to monitor arterial BP for >300 min, a period tenfold longer than reported in previous studies. The BP is recorded continuously and non-invasively, with an accuracy of 0.2 ± 4.5 mm Hg for diastolic pressures and 0.2 ± 5.8 mm Hg for systolic pressures, a performance equivalent to Grade A classification.

Monitoring blood flow is among the most basic practices of modern medicine. Blood carries essential fluids and passes through all organs, supplying them with oxygen and nutrients, removing waste and regulating temperature. The blood circulatory system can be considered a whole-body interconnecting organ; hence, malfunctions of other organs will be reflected in the blood flow, making it a vital health biomarker[1–4] for a variety of diseases, especially cardiovascular diseases that remain a leading cause of mortality worldwide[5]. Nevertheless, it is known that proactive and continuous monitoring of blood pressure (BP) can prevent fatalities associated with cardiovascular diseases[6–9]. In cases of sleep apnoea, stroke or hypertension, it is essential to monitor the patient's BP routinely and continuously to investigate disease development and treatment response[10–12]. Medical practitioners rely at present on traditional cuff sphygmomanometers, measuring static values of systolic (SBP), diastolic (DBP) and mean arterial (MAP) BP[13–15]. However, uninterrupted continuous monitoring of patients' haemodynamics[16–18] in daily, ambulatory and nocturnal settings cannot be achieved with the modern cuff sphygmomanometers[14,19] owing to their bulkiness and the discomfort caused by cuff inflation[3,20].

Directly capturing an individual's BP in a continuous manner is a non-trivial technological challenge. A few cuffless BP monitoring methods exist, relying on acoustic[21,22], pressure[23,24] or optical[25,26] modalities (Supplementary Table 1). The common drawbacks of the first two systems are their bulkiness and incompatibility with skin's elastic properties. The acoustic modalities utilizing ultrasound transducers can be miniaturized and packaged into smaller wearable patches[22], yet they are ~1,000 times thicker than graphene tattoos (Supplementary Table 1) and slide during movement, causing sensor displacement and thus requiring frequent recalibration. Although the ultrasound transducers can be made wearable, the ultrasound generators are bulky and hence cannot easily be incorporated into untethered ambulatory sensors[22]. For optical modalities, the principal drawback is the limited penetration of light into the tissue and their inability to capture haemodynamic parameters from arterial locations[27]. It has been proven that optical sensors can estimate heart rate from the skin surface and capillaries[25,26]; however, the BP pulse wave does not reach capillaries effectively[28], so BP cannot be captured from the capillaries (Supplementary Fig. 1).

Bioimpedance measurements (Bio-Z)[29–31], on the other hand, have the capability of buried tissue sensing through the deep penetration of electrical currents, facilitating robust sensing of haemodynamic parameters directly from arteries. Self-adhesive, low-impedance graphene electronic tattoos (GETs)[32–34] settle on the skin and sense from the same location over time; the BP estimation model for the tattoo placement is therefore determined at the outset, without the need to recalibrate the model for each electrode placement in contrast to other wearable electrode types[35]. Unlike previous works, the graphene-enabled BP (Z-BP) technology presented here does not suffer from electrode misplacement or sensor movement, and does not require the presence of bone. The self-adhesive, low-impedance GETs afford continuous BP measurement (>5 h, significantly longer than previous reports; Supplementary Table 2)[21,22,24] involving various activities, achieving accuracies of 0.2 ± 4.5 mm Hg (DBP), 0.2 ± 5.8 mm Hg (SBP) and 0.1 ± 5.3 mm Hg (MAP). The presented Z-BP technology (Fig. 1a) provides a unique and innovative solution that can advance wearable BP monitoring.

Graphene bioimpedance tattoos

To enable reliable Z-BP measurements, we placed a set of three GET pairs onto the wrist over the radial and ulnar arteries, both branching out of the brachial artery (Fig. 1b); the outer GETs were used to inject an alternating current (a.c. 0.2–1 mA) at 10 kHz into the tissue, and the inner pairs were used to record corresponding changes in the biopotentials. Frequency-dependent Bio-Z spectroscopy was performed (Supplementary Fig. 2) utilizing the custom-built circuit board (XL-board; see Methods and Supplementary Note 3) and the

[1]Department of Electrical and Computer Engineering, The University of Texas at Austin, Austin, TX, USA. [2]Microelectronics Research Center, The University of Texas, Austin, TX, USA. [3]Department of Electrical and Computer Engineering, Texas A&M University, College Station, TX, USA. [4]Department of Biomedical Engineering, Texas A&M University, College Station, TX, USA. [5]Department of Computer Science and Engineering, Texas A&M University, College Station, TX, USA. [6]These authors contributed equally: Dmitry Kireev, Kaan Sel. ✉e-mail: rjafari@tamu.edu; deji@ece.utexas.edu

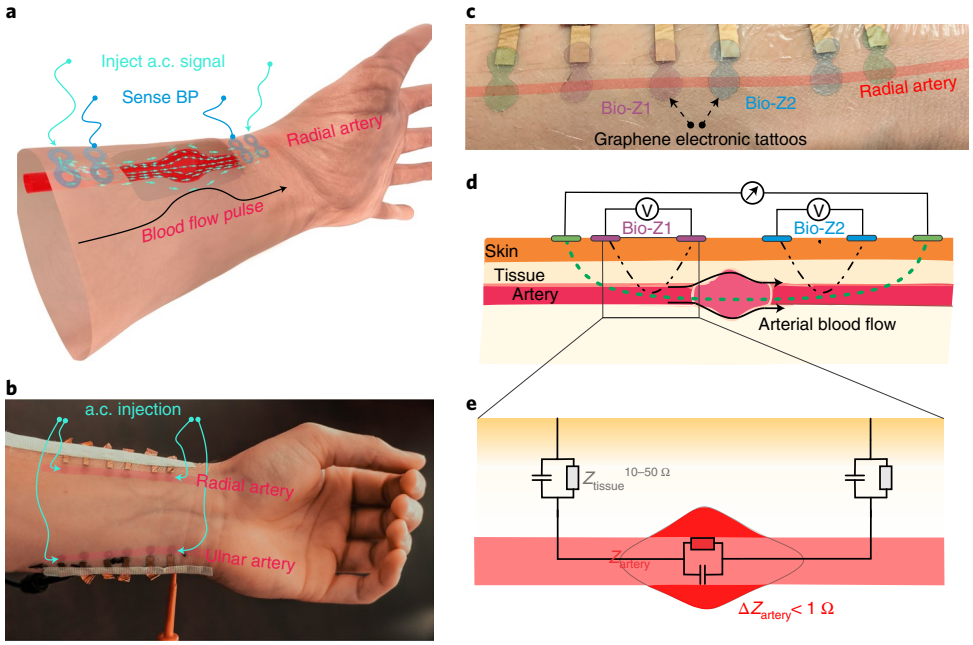

Fig. 1 | Illustration of Z-BP measurement modality. a, Three-dimensional schematic of the GETs placed onto the participant's wrist over the radial artery, with two outer tattoos used for a.c. injection, and two inner tattoos used to measure voltage changes. **b**, Photograph of 12 GETs, each with a surface area of 25 mm^2, placed on the radial (six tattoos, comprising Bio-Z1 and Bio-Z2) and ulnar (six tattoos, comprising Bio-Z3 and Bio-Z4) arteries on a participant's wrist. This multiplexed tattoo placement is essential for effective BP capture. The arteries are pseudo-coloured in pink for visibility, and their locations were tracked using an ultrasound vascular Doppler probe. **c**, Close-up view of six GETs at the radial artery. The injecting GETs are pseudo-coloured in green, the Bio-Z1 pair in violet and the Bio-Z2 pair in blue, as the graphene is almost invisible. **d**, Cross-section of the six GETs, with green lines representing the a.c. injected signal and grey lines representing voltage sensing. **e**, Close-up view of one pair of sensing GETs and the simplified equivalent electrical circuit of the interface, showing Z_{tissue} and Z_{artery}, part of which (ΔZ_{artery}) is related to the undulating blood volume. Credit: **a**, Jo Wozniak, Texas Advanced Computing Center.

current injection frequency and amplitudes were chosen deliberately to mitigate the effect of $1/f$ noise, where f is the frequency, and to adhere to the safety standards of current injection into a human body (Supplementary Fig. 3)[36]. The non-invasive signal at high frequencies (as high as 1 mA at 10 kHz according to safety standards[36]; Supplementary Note 8) penetrated deep into the tissue along the path of least impedance on its course[37]. The rich ionic solution in the blood vessels acts as a better conductor than the surrounding fat and muscle cells, hence the artery is the prevailing lowest-resistance path for the injected a.c. signal (Fig. 1a–c). The electrode placement configuration and the corresponding electrode–skin–artery simplified electrical diagram are shown in Fig. 1d,e. The Bio-Z method[38] is similar to the conventional four-probe resistance measurement (that is, the Kelvin probe) of electronic materials[39]. It affords separation of the contact (skin–electrode, $Z_{S\text{-}E} \approx 1\text{–}10\,k\Omega$) and tissue ($Z_{tissue} \approx 10\text{–}50\,\Omega$) impedances from the desired arterial bioimpedance ($Z_{artery} \approx 1\,\Omega$, Fig. 1e), and only the latter two were detected by the sensing electrodes. The acquired signal was bandpass-filtered and demodulated (Supplementary Fig. 4 and Methods). The variable part of the bioimpedance ($\Delta Z_{artery}(t) < 50\,m\Omega$) represents the blood volume undulations in the artery due to pulse pressure waves. Our low-noise multichannel sensing hardware (Methods) allowed us to detect bioimpedance with an accuracy down to 1 mΩ. Furthermore, specific emphasis on the fast pulsatile changes in bioimpedance enabled us to disregard the slow variations in the tissue and blood composition as a result of participants' daily consumption of food or water (Supplementary Fig. 5). The high-frequency sensing (10 kHz) allowed us to bypass the undesirable influence of surface potentials such as electromyography (EMG, Supplementary Fig. 4).

The actual blood pulse waveform is directly associated with the blood flow, its dynamics and arterial volume (Fig. 2a)[40]. The lowest pressure (~70 ± 10 mm Hg at rest for healthy individuals) is the so-called DBP. The highest built-up pressure is recognized as the SBP (~120 ± 10 mm Hg at rest for healthy individuals). The arterial volume is then inversely proportional to $\Delta Z_{artery}(t)$. The general trend is that higher BP results in higher arterial volume, and accordingly lower bioimpedance. Therefore, the Bio-Z waveform (shown in Fig. 2b) is reciprocal to the BP. Moreover, BP is also correlated with the blood pressure wave velocity (PWV, V_{PW}) passing through the arteries. The relationship between V_{PW} and BP theoretically builds upon models that include the artery's elastic properties (Supplementary Note 5)[41]. V_{PW} was obtained by measuring the pulse transit time (PTT, t_{pt}) between two arterials sites (that is, V_{PW} is proportional to $1/t_{pt}$); Bio-Z must therefore be measured from at least two locations, which was accomplished by placing two pairs of signal-sensing GETs per artery. Moreover, multiple PTTs were extracted using the time difference between the arrival of pulses to the radial and ulnar arteries. The ΔZ_{artery} values were used to identify the four characteristic points (systolic foot, diastolic peak, mean slope and inflection point, as shown in Fig. 2c) and used to build the machine learning regression algorithm for BP estimation (Methods and Supplementary Note 5). Here, the machine learning model created the mapping between characteristic features extracted from Bio-Z waveforms and BP, involving a multi-variable nonlinear mathematical framework. To keep the dimensions of the wearable sensor suitable for measurement, the spacing between the two outer injection electrodes was set to 40 mm, while all other electrodes were placed as close as possible, typically about 8 mm apart (Supplementary Fig. 6).

The GETs were fabricated according to our published protocol (Methods)[34], and were based on chemical-vapour-deposited (CVD) graphene with large-area uniformity, optical transparency and reliable electrical properties. In this work, we used few-layer GET structures that provided superior electrical properties while conforming

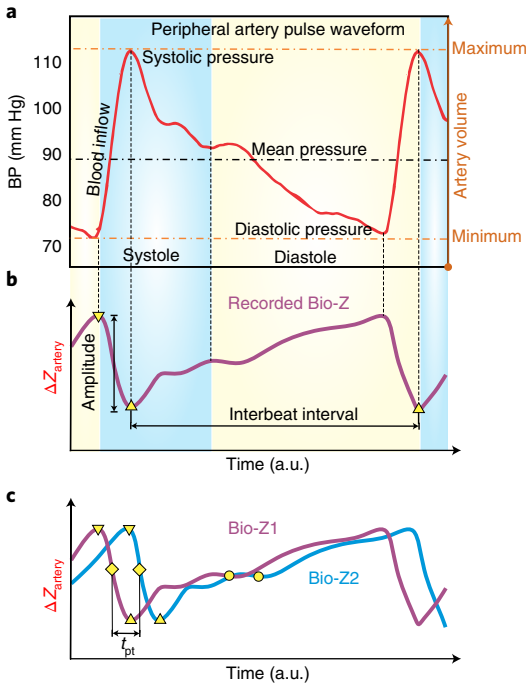

Fig. 2 | Correlation between arterial BP and bioimpedance. a, Illustration of the peripheral arterial BP pulse waveform (red) and correlated arterial volume[40]. The systole and diastole BP regions are highlighted in blue and yellow, respectively. **b**, The Bio-Z signal (violet) is reciprocal to the BP pulse waveform. **c**, Two Bio-Z signals recorded by two pairs of GETs are essential for calculating t_{pt} and the interbeat interval, which are used for the machine learning algorithm. The complete machine learning regression analysis is based on four main features: the systolic and diastolic phases (upward and downward triangles), the maximum slope (rhombus) and the inflection point (circle).

closely to the skin and fault-free long-term operation[34]. All sensing pairs of tattoos were made of bilayer GETs (2L-GETs), and injection electrodes were made of trilayer GETs (3L-GETs) with superior impedance properties (Supplementary Fig. 7). The 3L-GETs were chosen for the current injection electrodes as they provided (1) lower interface impedance, as required to inject the highest possible a.c. signal, and (2) lower variability compared with previously reported monolayer GETs[32,33]. The latter is essential mainly for the current injection electrodes, and the 3L-GETs featured superior consistency (Supplementary Fig. 7a). The tattoo transfer process is rapid and can be scaled up (Supplementary Video 2). The mechanical properties of multilayer GETs are not much different from those of monolayer GETs[32,42]. To verify their longevity and durability, the 2L-GETs were subjected to continuous stress when worn directly on a person throughout their routine daily activities, and the impedance was monitored constantly (Supplementary Fig. 7e). It could be seen that the performance of the 2L-GET did not degrade over hours of desktop work and light walking. Even when performing activities demanding substantial wrist bending, the tattoo–skin interface impedance changed by only ~20%. Upon strenuous exercise (for example, push-ups), the impedance rose by ~45%, indicating that GETs can endure normal stretching of the skin and are advantageous for long-term Bio-Z experiments. The GETs survived even a challenging water immersion test (Supplementary Video 1).

Graphene blood pressure measurement results

The BP data were gathered from $N=7$ healthy individuals (more participants than previous works on emerging BP sensors[21,22,24]) in their mid-twenties with institutional review board approval. No individuals with hypertension were specifically selected for this proof-of-concept study. Thirteen GETs were placed onto each of the participant's wrists: six on each artery (two injecting and four sensing), and one reference GET. Over 100 pairs of identical GETs were used for testing and calibration, ensuring rigorous BP monitoring within this work. No skin irritation, damage, allergic reaction or redness were observed in GET–skin observations.

To capture the graphene Z-BP, the Bio-Z signals must be cross-correlated with the participant's BP across a wide range. The participants thus performed various exercise manoeuvres to intentionally elevate their BP; namely, hand grip and cold pressor (HGCP), cycling on a stationary bicycle, and Valsalva manoeuvre (Supplementary Fig. 8). The first two routines elevate BP due to physical exercise, and the Valsalva manoeuvre is a classic clinical procedure to induce a rapid rise in BP due to the build-up of internal lung pressure[43]. The majority of the participants ($N=6$) performed a series of HGCP manoeuvres to elevate their BP gradually. After the initial baseline recording at rest, the participants exercised with a hand grip for 3 min, slowly raising their BP. To ensure an equally slow BP drop after finishing the exercise, the participants immersed their right hands into a bucket of ice-cold water for 1 min (Fig. 3a), a procedure known as the cold pressor test[44]. Following a resting period of ~3–4 min, the HGCP routine (Supplementary Fig. 8) was repeated. A medical-grade BP monitoring device, Finapres NOVA, was used to measure the participant's control BP during the experiments. On average, each participant underwent 4 ± 1 h of continuous BP monitoring. In total, we performed on average ~$2{,}500\pm600$ BP measurements per participant, which resulted in a total of 18,667 data points (Supplementary Tables 2–9). It is worth noting that to obtain clean reference BP recordings with the Finapres NOVA and acquire high-fidelity bioimpedance signals, our experimental routine was designed cautiously to minimize motion artefacts (Supplementary Videos 3 and 4).

Blood pressure model training and performance evaluation

The HGCP manoeuvre-induced patterns of DBP, SBP and MAP as measured via the GETs for one participant are shown in Fig. 3c. The same time traces of HGCP routines for all other participants can be seen in Supplementary Fig. 9. It is apparent that BP manoeuvres allow us to raise the DBP and SBP over broad ranges of 50–120 mm Hg and 100–180 mm Hg, respectively. Figure 3b shows the scatter plot of the Z-BP yielded from all six participants via HGCP-enabled training, covering DBP in the range of 50–120 mm Hg and SBP in the range of 100–180 mm Hg, which is normal for healthy individuals during exercise. For one participant, the DBP and SBP values reached ~130 mm Hg and ~200 mm Hg, respectively. Such high BP might otherwise be considered hypertensive; however, they were only reached for a short time during exhaustive exercise by a non-athlete; as such, it is considered normal[45]. The histogram plots of the DBP and SBP distributions for all participants can be found in Supplementary Figs. 10 and 11. Similar experiments were performed with a wristband of conductive dry metal Ag electrodes on the same participant (Fig. 3d). As can be seen, the graphene-enabled Z-BP features much better accuracy than the Ag wristband. According to the IEEE standard for wearable BP measuring devices[46], the absolute mean error (m.e.) and standard deviation of the error (s.d.) are used here as the major figures of merit (m.e. $\pm$ s.d.), with additional standard deviations and 95% confidence intervals provided in Supplementary Tables 4–9 for a better view of the data. The overall m.e. and s.d. of BP monitoring via GETs are 0.2 ± 4.5 mm Hg (DBP) and 0.2 ± 5.8 mm Hg (SBP), compared with the values for the Ag wristband of 0.5 ± 5.0 mm Hg (DBP) and 0.5 ± 7.4 mm Hg (SBP). As per the IEEE standard[46], the performance can be categorized as comparable to Grade A, the highest level of accuracy (Fig. 3e and Supplementary Fig. 12). Although

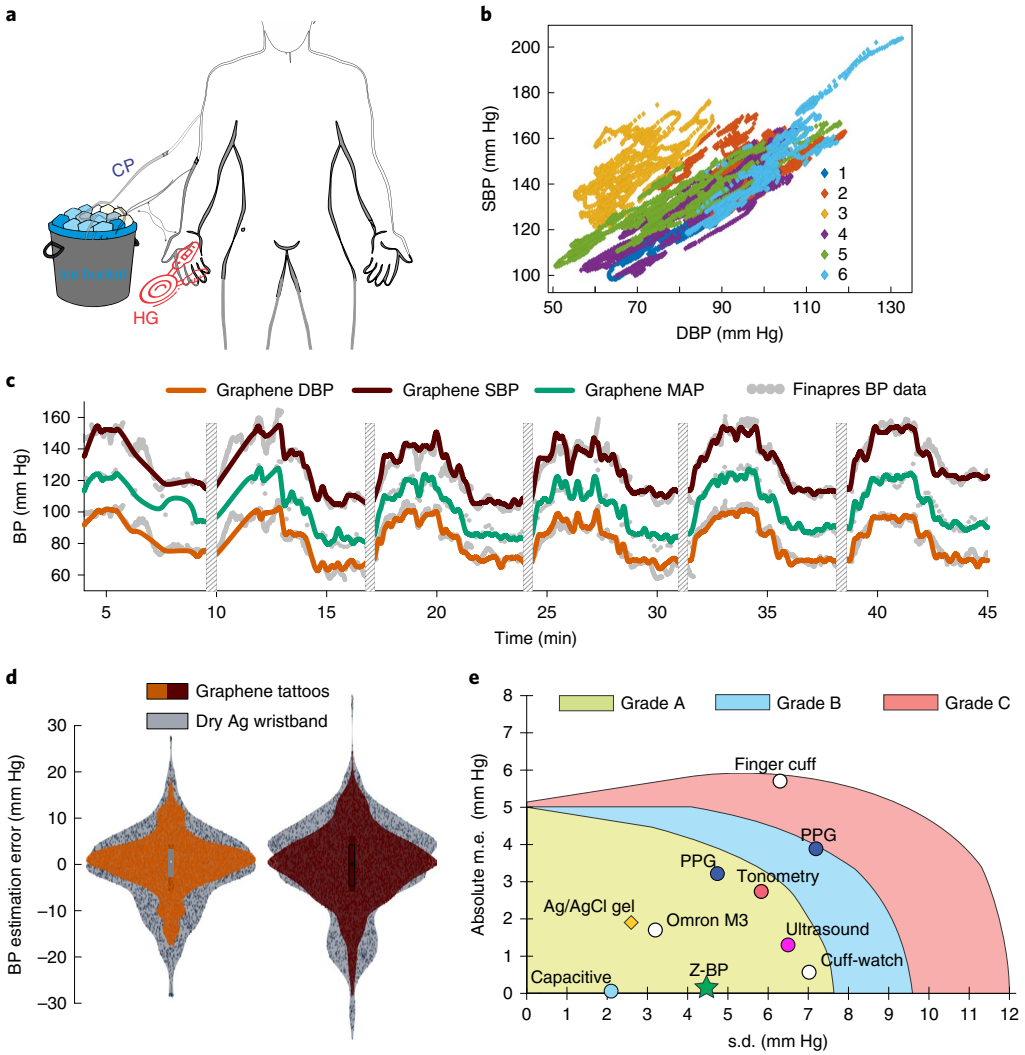

Fig. 3 | Graphene Z-BP measurement results from the HGCP routine. a, Illustration of the HGCP routine that was performed by participants with their right hands. An array of 13 GETs, over radial and ulnar arteries, were placed on the participants' left forearms. **b**, Scatter diagram of all DBP and SBP values from six participants, indicating the wide dynamic BP range coverage that is essential for effective BP prediction. **c**, Six consecutive HGCP-induced BP manoeuvres: DPB, SBP and MAP as measured via the GETs and correlated with the control BP (Finapres NOVA). The dashed areas indicate short (~10 min) breaks between the sets of HGCP manoeuvres. The graphene Z-BP time trace is closely correlated with the control BP. **d**, The statistical violin plots for graphene Z-BP (DBP (left) and SBP (right)) given in direct comparison with Ag wristband-derived BP (grey) from the same participant. The plot indicates that the accuracy of graphene-enabled BP monitoring is superior to that of the dry Ag wristband. The violin plot includes the box plot (defined as Q1 and Q3 quartiles, and median) with a kernel density estimation over the points. **e**, Comparison of the DBP estimation accuracy achieved with the GETs (Z-BP, green star) with Ag/AgCl gel-based BP[35], photoplethysmography (PPG)[25], ultrasound[52], tonometry[53], capacitive sensors[24] and various cuff-based methods (white circles)[54,55]. Only the works with relevant (m.e. and s.d.) data provided were included. The background shading shows the IEEE accuracy categories (Grades A, B and C)[46].

the time trace (Fig. 3c) shows a slight deviation in Z-BP from the control BP, this represents long-term visualization of an emergent technology capable of high-speed and long-term (>45 min) continuous sampling of an individual's BP with the highest accuracy. The Ag electrode wristband is also a bulky and intrusive device (Supplementary Fig. 13), imposing extensive forces on the skin to gain reliable recordings, and is therefore unsuitable for long-term monitoring.

It is worth noting that the six participants of different ages performing the HGCP exercises had different body mass index (BMI) values, and we found no dependency between the Z-BP estimation accuracy and BMI (*t*-test: $P < 0.05$, Supplementary Fig. 14), indicating that Z-BP modality provides Grade A accuracy regardless of the experimental BMI range. In alternative exercises for BP elevation, five participants performed the Valsalva manoeuvre, and another participant performed treadmill cycling (Supplementary Fig. 15). It is evident that (Fig. 4a), in contrast to HGCP, cycling provides a shallow and less valuable data range for DBP and SBP: 55–75 mm Hg and 100–140 mm Hg, respectively. The Valsalva manoeuvre, on the other hand, with a much lower number of data points (the routine itself is quick), covers a reasonably wide range of the DBP and SBP: 60–120 mm Hg and 110–180 mm H (ref. [43]).

Besides the aforementioned experimental routines for elevating BP, we used different machine learning models of data regression[47] with adaptive boosting (AdaBoost, see Methods) as the basic technique[35]. AdaBoost handles ~50 features extracted from four Bio-Z signals (Fig. 2c, Methods and Supplementary Note 5) to train the machine learning algorithm. During training, these features were correlated with the control BP (measured via Finapres NOVA, see Supplementary Note 9) and the hidden network of decision trees

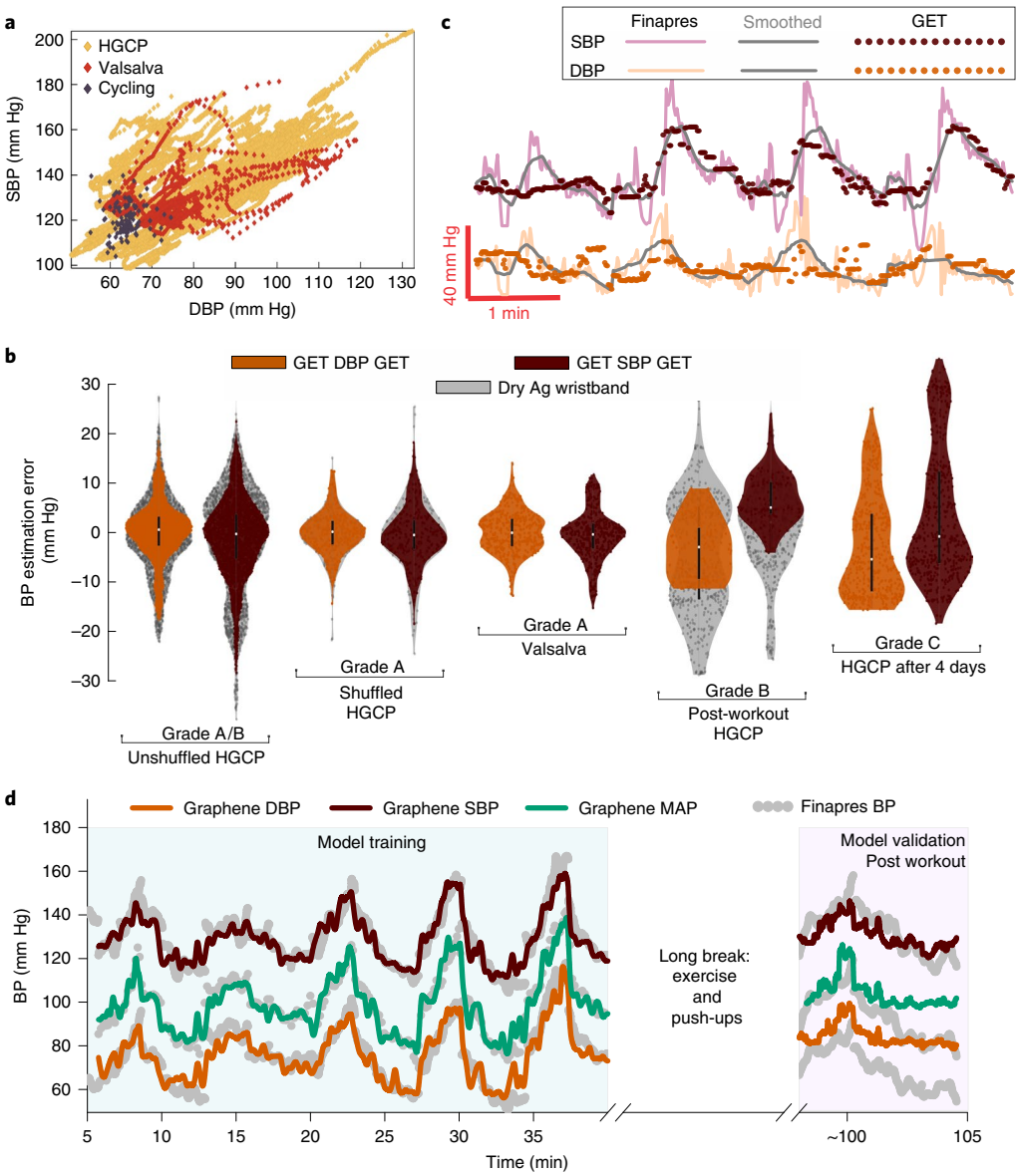

Fig. 4 | Graphene Z-BP model training and performance evaluation. a, DBP and SBP scatter plots for three BP elevation manoeuvres of: HGCP, the Valsalva manoeuvre and cycling. HGCP is a time-consuming routine but raises BP in a usefully wide range; cycling is less effective at elevating BP and the Valsalva manoeuvre is equally effective as HGCP, with a considerably lower number of training points. **b**, Violin plots representing the accuracies of graphene Z-BP compared with Ag wristbands for different machine learning routines: shuffled HGCP, unshuffled HGCP, Valsalva, post-workout and after a 4 day break. The shuffled HGCP and Valsalva based models yielded the lowest median error of BP estimation. The violin plots include box plots (defined as Q1 and Q3 quartiles, and median) with a kernel density estimation over the points. The corresponding accuracy categories are labelled. **c**, A time trace of BP changes during three consecutive Valsalva manoeuvres, measured via Finapres NOVA, smoothed with an average window of 20 heartbeats as necessary for accurate machine learning training and as predicted via graphene-enabled Z-BP recordings. Each Valsalva cycle has two peaks and one dip in BP. However, the smoothing algorithm results in waveform alteration and a less pronounced dip. **d**, Time trace of DBP, SBP and MAP changes for one participant during a series of HGCP exercises as measured by GETs compared with the control BP, followed by an hour-long break including a workout and the model validation session with another HGCP pattern.

selected the best correlation features to follow. The training is typically done on shuffled HGCP data (Supplementary Fig. 16 and Methods); the original time trace is shuffle and split into ten equal parts. One part is then used for training and nine for testing, repeated ten times (that is, tenfold cross-validation analysis). The implementation of tenfold cross-validation allows the machine learning model to leverage a significant portion of the training data and avoid overfitting. After the training, the data were rearranged in the original time order. The shuffled machine learning algorithm for GET-enabled Z-BP results in accuracies of 0.2 ± 4.5 mm Hg (DBP), 0.2 ± 5.8 mm Hg (SBP) and 0.1 ± 5.3 mm Hg (MAP), categorizing it as comparable to Grade A[46]. The same machine learning technique was used on the same data but without shuffling (Fig. 4b), meaning that the algorithm can be used online, during the data collection process, thereby accelerating the learning process. This algorithm results in lower accuracies of 0.07 ± 7.15 mm Hg (DBP, Grade A) and 0.01 ± 8.9 mm Hg (SBP, Grade B), but still outperforms the Ag wristband (Fig. 4b).

Figure 4c shows the time trace of three Valsalva manoeuvre patterns performed consecutively, as measured via GETs and corroborated with the Finapres NOVA. Surprisingly, the rapid Valsalva

training exercise with a low number of training data points yields noteworthy accuracies of 0.8 ± 6.1 mm Hg (DBP), 0.5 ± 6.9 mm Hg (SBP) and 0.3 ± 5.3 mm Hg (MAP), indicating that such a rapid routine could be used for reliable and accurate (Grade A) model training in the future. The time-consuming cycling training routine also resulted in superior BP estimation accuracies of 0.06 ± 2.5 mm Hg (DBP), 0.2 ± 3.6 mm Hg (SBP) and 0.0 ± 6.6 mm Hg (MAP) of the graphene Z-BP (Grade A), outperforming even medical-grade gel electrodes (Supplementary Table 1)[35]. The superb accuracy of BP estimation via cycling-enabled training can be explained by the shallow range of elevated BP during such exercise (not capturing elevated BP). The shallow BP range coupled with excessive motion during exercise makes cycling less suitable for actual model training in ambulatory conditions.

The main innovation of this work is the discovery that GETs in combination with bioimpedance can be used for continuous monitoring of BP in wearable and ambulatory conditions. This implies that participants can move freely and perform daily activities. In this context, after the HGCP training routines were complete, all participants were assigned to perform a set of activities (for example, walking, eating and strenuous workouts). Some selected participants went through an extensive sweat-inducing walk outside at 38 °C and others performed push-ups. It is worth noting that the GETs did not degrade electrically after exposure to light and heat or contact with water or sweat. After a workout, the participants came back for post-exercise BP monitoring using the pre-built machine learning algorithm. The post-workout accuracy was slightly worse and the confidence interval was wider (Fig. 4b). Nonetheless, the overall accuracies achieved (3.6 ± 6.2 mm Hg for DBP and 1.65 ± 8.5 mm Hg for SBP) were comparable to Grade B of the IEEE standard[46]. Similar measurements were performed with the Ag wristband electrodes, yielding substantially inferior accuracies (Fig. 4b). The time traces of BP evolution for one participant going through a series of HGCP training events, then an hour-long break for eating and push-ups, followed by the repetition of a single HGCP pattern using the pre-trained model for BP validation can be found in Fig. 4d.

Furthermore, to highlight the advantages of our Z-BP modality, one participant's BP model was built upon the training routine performed on day 1. The participant was then sent home and was free to perform daily activities for three days. On day 4, another set of identical GETs were transferred to the same participant and BP was estimated using the pre-built machine learning calibration data, while the control BP was recorded to corroborate the results. It was found that such a generic pre-built algorithm model for a participant can be reused, providing sufficient (Grade C)[46] accuracies of 4.6 ± 8.3 mm Hg (DBP) and 0.8 ± 11.8 mm Hg (SBP) (Fig. 3e and Supplementary Fig. 12). Such reuse is not possible with Ag/AgCl gel electrodes due to the large displacement of the electrodes over time, mechanical instability and drying[35].

Besides extracting the essential BP features, the raw Bio-Z is rich with additional data that can be used to monitor other vital signs, such as breathing respiration rate[30]. Breathing is facilitated by lung volume increase, which in turn imposes undulating internal pressure onto surrounding objects, exerting a substantial influence on arterial BP[30,37,48]. Supplementary Fig. 17 summarizes the Bio-Z extracted respiration rate data, fast Fourier transformation analysis and time trace of the respiration rate changes measured continuously with no additional signal recording. The same data used for BP estimation were used for respiration rate monitoring with a different post-processing algorithm (Methods and Supplementary Table 10).

Graphene Z-BP can be measured from any artery. Hence, we recorded the Bio-Z signals from the tibial and carotid arteries and the jugular notch (Supplementary Fig. 18). Estimating BP from other arteries, especially those nearest to the heart, means that the central BP is recorded, which differs from the peripheral BP and bears additional useful information[49]. However, recording the central BP requires clinical studies and a catheter-based reference, which is highly invasive, but could be investigated in future clinical studies. Recording brachial BP from the wrist is technologically promising for next-generation soft wearable technologies. The dimensions of the designed tattoo array are thus within the size of modern wristwatches, making translation into a fully wearable technology possible in the future.

Conclusions

To conclude, we demonstrate an innovative proof-of-concept bioimpedance platform to measure BP and blood flow by leveraging GETs that enable intimate location-stable contact with skin, yielding an accuracy that exceeds previous reports. The accuracies of our Z-BP method were 0.06 ± 2.5 mm Hg (DBP) and 0.2 ± 3.6 mm Hg (SBP) for a cycling-trained machine learning regression model, and 0.2 ± 4.5 mm Hg (DBP) and 0.2 ± 5.8 mm Hg (SBP) when an HGCP training routine was used. According to the IEEE standard, these values are equivalent to Grade A wearable BP measuring devices[46]. Hence, the accuracies of graphene Z-BP reported in this work, even post-workout, are suitable for accurate continuous BP monitoring. The reported graphene Z-BP outperforms contemporary Ag wristband electrodes and wet Ag/AgCl gel electrodes (Supplementary Table 1). The significant advantage of leveraging GETs for the task is their intimate conformal contact with the skin (Supplementary Figs. 19 and 20), requiring only a primary calibration and subsequent continuous usage. Furthermore, our system demonstrates a capacity to run nocturnally with high fidelity without disturbing patients, which is not feasible with current obtrusive cuff-based monitors[3,50,51] or low-fidelity emerging cuffless BP monitoring solutions[25,26] owing to motion-noise artefacts that decrease the machine learning model efficiency[35]. Deployment of the system with miniaturized integrated circuits, wireless operation and data storage capabilities in the context of a smart-watch solution are among the future steps for translational research to develop a fully integrated wearable system.

Online content

Any methods, additional references, Nature Research reporting summaries, source data, extended data, supplementary information, acknowledgements, peer review information; details of author contributions and competing interests; and statements of data and code availability are available at https://doi.org/10.1038/s41565-022-01145-w.

Received: 8 September 2021; Accepted: 3 May 2022;
Published online: 20 June 2022

References

1. Jennings, J. R., Muldoon, M. F., Allen, B., Ginty, A. T. & Gianaros, P. J. Cerebrovascular function in hypertension: does high blood pressure make you old? *Psychophysiology* **58**, 1–17 (2021).
2. Shaffer, F., McCraty, R. & Zerr, C. L. A healthy heart is not a metronome: an integrative review of the heartas anatomy and heart rate variability. *Front. Psychol.* **5**, 1040 (2014).
3. Kwon, Y. et al. Blood pressure monitoring in sleep: time to wake up. *Blood Press. Monit.* **25**, 61–68 (2020).
4. Magder, S. The meaning of blood pressure. *Crit. Care* **22**, 257 (2018).
5. Benjamin, E. J. et al. Heart disease and stroke statistics—2019 update: a report from the American Heart Association. *Circulation* **139**, e556–e528 (2019).
6. Flint, A. C. et al. Effect of systolic and diastolic blood pressure on cardiovascular outcomes. *N. Engl. J. Med.* **381**, 243–251 (2019).
7. Kario, K. Management of hypertension in the digital era. *Hypertension* **76**, 640–650 (2020).
8. Carey, R. M., Muntner, P., Bosworth, H. B. & Whelton, P. K. Prevention and control of hypertension. *J. Am. Coll. Cardiol.* **72**, 1278–1293 (2018).
9. Kario, K. et al. Morning home blood pressure is a strong predictor of coronary artery disease: the honest study. *J. Am. Coll. Cardiol.* **67**, 1519–1527 (2016).

10. Al Ghorani, H., Kulenthiran, S., Lauder, L., Böhm, M. & Mahfoud, F. Hypertension trials update. *J. Hum. Hypertens.* **35**, 398–409 (2021).
11. Marrone, O. & Bonsignore, M. R. Blood-pressure variability in patients with obstructive sleep apnea: current perspectives. *Nat. Sci. Sleep.* **10**, 229–242 (2018).
12. Salazar, M. R. et al. Nocturnal hypertension in high-risk mid-pregnancies predict the development of preeclampsia/eclampsia. *J. Hypertens.* **37**, 182–186 (2018).
13. Stergiou, G. S. et al. A universal standard for the validation of blood pressure measuring devices. *Hypertension* **71**, 368–374 (2018).
14. Bartels, K., Esper, S. A. & Thiele, R. H. Blood pressure monitoring for the anesthesiologist. *Anesth. Analg.* **122**, 1866–1879 (2016).
15. Vischer, A. S. & Burkard, T. Principles of blood pressure measurement – current techniques, office vs ambulatory blood pressure measurement. *Adv. Exp. Med. Biol.* **956**, 85–96 (2016).
16. Siu, A. L. et al. Screening for high blood pressure in adults: U.S. preventive services task force recommendation statement. *Ann. Intern. Med.* **163**, 778–786 (2015).
17. Jeong, I. C., Bychkov, D. & Searson, P. C. Wearable devices for precision medicine and health state monitoring. *IEEE Trans. Biomed. Eng.* **66**, 1242–1258 (2019).
18. Li, R., Liang, N., Bu, F. & Hesketh, T. The effectiveness of self-management of hypertension in adults using mobile health: systematic review and meta-analysis. *JMIR mHealth uHealth* **8**, e17776 (2020).
19. \Asayama, K., Ohkubo, T. & Imai, Y. In-office and out-of-office blood pressure measurement. *J. Hum. Hypertens*. https://doi.org/10.1038/s41371-021-00486-8 (2021).
20. Pandit, J. A., Lores, E. & Batlle, D. Cuffless blood pressure monitoring. *Clin. J. Am. Soc. Nephrol.* **15**, 1531–1538 (2020).
21. Wang, C. et al. Monitoring of the central blood pressure waveform via a conformal ultrasonic device. *Nat. Biomed. Eng.* **2**, 687–695 (2018).
22. Wang, C. et al. Continuous monitoring of deep-tissue haemodynamics with stretchable ultrasonic phased arrays. *Nat. Biomed. Eng.* **5**, 749–758 (2021).
23. Luo, N. et al. Flexible piezoresistive sensor patch enabling ultralow power cuffless blood pressure measurement. *Adv. Funct. Mater.* **26**, 1178–1187 (2016).
24. Kim, J. et al. Soft wearable pressure sensors for beat-to-beat blood pressure monitoring. *Adv. Healthc. Mater.* **8**, 1–9 (2019).
25. Yang, S., Zhang, Y., Cho, S. Y., Correia, R. & Morgan, S. P. Non-invasive cuff-less blood pressure estimation using a hybrid deep learning model. *Opt. Quantum Electron.* **53**, 1–20 (2021).
26. Elgendi, M. et al. The use of photoplethysmography for assessing hypertension. *npj Digit. Med.* **2**, 1–11 (2019).
27. Chang, Y. H., Huang, K. C., Yang, C. C. & Tsai, H. Y. Evaluation of absorbed light dose in human skin tissue during Light Therapy by 630nm LED light. In *2015 IEEE 12th International Conference on Networking, Sensing and Control* 394–398 (IEEE, 2015); https://doi.org/10.1109/ICNSC.2015.7116069
28. Safar, M. E. & Boudier, H. S. Vascular development, pulse pressure, and the mechanisms of hypertension. *Hypertension* **46**, 205–209 (2005).
29. Sel, K. et al. Electrical characterization of graphene-based e-tattoos for bio-impedance-based physiological sensing. In *2019 IEEE Biomedical Circuits and Systems Conference* 1–4 (IEEE, 2019); https://doi.org/10.1109/BIOCAS.2019.8919003
30. Sel, K., Osman, D. & Jafari, R. Non-invasive cardiac and respiratory activity assessment from various human body locations using bioimpedance. *IEEE Open J. Eng. Med. Biol.* **2**, 210–217 (2021).
31. Wang, T. W., Chen, W. X., Chu, H. W. & Lin, S. F. Single-channel bioimpedance measurement for wearable continuous blood pressure monitoring. *IEEE Trans. Instrum. Meas.* **70**, 1–9 (2021).
32. Kabiri Ameri, S. et al. Graphene electronic tattoo sensors. *ACS Nano* **11**, 7634–7641 (2017).
33. Ameri, S. K. et al. Imperceptible electrooculography graphene sensor system for human–robot interface. *npj 2D Mater. Appl.* **2**, 19 (2018).
34. Kireev, D. et al. Fabrication, characterization and applications of graphene electronic tattoos. *Nat. Protoc.* **16**, 2395–2417 (2021).
35. Ibrahim, B. & Jafari, R. Cuffless blood pressure monitoring from an array of wrist bio-impedance sensors using subject-specific regression models: proof of concept. *IEEE Trans. Biomed. Circ. Syst.* **13**, 1723–1735 (2019).
36. American National Standards Institute, Association for the Advancement of Medical Instrumentation. ANSI/AAMI ES60601-1:2005/A1:2012, Medical Electrical Equipment Part 1: General Requirements for Basic Safety and Essential Performance (ANSI/AAMI 2012); https://webstore.ansi.org/Standards/AAMI/ansiaamies606012005r2012
37. Sel, K., Ibrahim, B. & Jafari, R. ImpediBands: body coupled bio-impedance patches for physiological sensing proof of concept. *IEEE Trans. Biomed. Circ. Syst.* **14**, 757–774 (2020).
38. Webster, J. *Medical Instrumentation: Application and Design* 4th edn (John Wiley & Sons, 2010).
39. Miccoli, I., Edler, F., Pfnür, H. & Tegenkamp, C. The 100th anniversary of the four-point probe technique: the role of probe geometries in isotropic and anisotropic systems. *J. Phys. Condens. Matter* **27**, 223201 (2015).
40. Brath, P. C. & Eisenach, J. C. Atlas of cardiovascular monitoring. *Anesthesiology* **93**, 312–312 (2000).
41. Vlachopoulos, C., O'Rourke, M. & Nichols, W. W. *McDonald's Blood Flow in Arteries* (CRC, 2011); https://doi.org/10.1201/b13568
42. Jang, H., Dai, Z., Ha, K.-H., Ameri, S. K. & Lu, N. Stretchability of PMMA-supported CVD graphene and of its electrical contacts. *2D Mater.* **7**, 014003 (2019).
43. Goldstein, D. S. & Cheshire, W. P. Beat-to-beat blood pressure and heart rate responses to the Valsalva maneuver. *Clin. Auton. Res.* **27**, 361–367 (2017).
44. Johnson, B. D., Sackett, J. R., Schlader, Z. J. & Leddy, J. J. Attenuated cardiovascular responses to the cold pressor test in concussed collegiate athletes. *J. Athl. Train.* **55**, 124–131 (2020).
45. Byambasukh, O., Snieder, H. & Corpeleijn, E. Relation between leisure time, commuting, and occupational physical activity with blood pressure in 125 402 Adults: the Lifelines cohort. *J. Am. Heart Assoc.* **9**, e014313 (2020).
46. IEEE Engineering in Medicine and Biology Society *IEEE Standard for Wearable, Cuffless Blood Pressure Measuring Devices* IEEE 1708-2014 (IEEE, 2014).
47. Koshimizu, H., Kojima, R. & Okuno, Y. Future possibilities for artificial intelligence in the practical management of hypertension. *Hypertens. Res.* **43**, 1327–1337 (2020).
48. Herakova, N., Nwobodo, N. H. N., Wang, Y., Chen, F. & Zheng, D. Effect of respiratory pattern on automated clinical blood pressure measurement: an observational study with normotensive subjects. *Clin. Hypertens.* **23**, 15 (2017).
49. McEniery, C. M., Cockcroft, J. R., Roman, M. J., Franklin, S. S. & Wilkinson, I. B. Central blood pressure: current evidence and clinical importance. *Eur. Heart J.* **35**, 1719–1725 (2014).
50. Asayama, K. et al. Nocturnal blood pressuremeasured by home devices: Evidence and perspective for clinical application. *J. Hypertens.* **37**, 905–916 (2019).
51. Gaffey, A. E., Schwartz, J. E., Harris, K. M., Hall, M. H. & Burg, M. M. Effects of ambulatory blood pressure monitoring on sleep in healthy, normotensive men and women. *Blood Press. Monit.* **26**, 93–101 (2021).
52. Soleimani, E., Mokhtari-Dizaji, M., Fatouraee, N. & Saberi, H. Assessing the blood pressure waveform of the carotid artery using an ultrasound image processing method. *Ultrasonography* **36**, 144–152 (2017).
53. Kemmotsu, O. et al. Blood pressure measurement by arterial tonometry in controlled Hypotension. *Anesth. Analg.* **73**, 54–58 (1991).
54. Lee, J. Y., Choi, E. Y., Jeong, H. J., Kim, K. H. & Park, J. C. Blood pressure measurement using finger cuff. *Conf. Proc. IEEE Eng. Med. Biol. Soc.* **7 S**, 3575–3577 (2005).
55. Mazoteras Pardo, V., Losa Iglesias, M. E., López Chicharro, J. & Becerro de Bengoa Vallejo, R. The QardioArm app in the assessment of blood pressure and heart rate: reliability and validity study. *JMIR mHealth uHealth* **5**, e198 (2017).

Methods

GET fabrication. GET fabrication began with CVD growth of graphene on a copper foil or the purchase of CVD-grown graphene. To serve as a protective and permanent support layer, an ultrathin 200-nm-thick layer of polymethyl methacrylate (PMMA) was spin-coated on top of the graphene/Cu foil. Following a hard bake of the PMMA at 200 °C for 20 min, the stack was placed into a 0.1 M ammonium persulfate solution to etch the copper overnight. The PMMA/graphene stack was then transferred into fresh deionized water to clean the interface of the chemical residues. The process was repeated at least three times to ensure the complete removal of contaminants. Once ready, the PMMA/graphene stack was finally transferred onto the temporary tattoo paper[32,34]. The tattoo paper consisted of a specific resin-based coating that is slippery and anti-adhesive whenever wet, yet adhesive when dry. After the transfer and overnight drying, the graphene/PMMA/tattoo paper stack was loaded into a mechanical plotter that cuts a specific shape for the future GET devices. After the cut was performed, the excess graphene/PMMA was removed, and the tattoo could then be transferred onto the skin.

Two graphene/copper pieces were required to fabricate a 2L-GET[34]. PMMA was spin-coated onto the first piece (A) and hard-baked at 200 °C for 20 min, while the second piece (B) was left pristine. Piece A was placed into copper etchant, then transferred into a deionized water cascade after the etch was complete (same procedure as before). This time, however, the bare piece (B) was used to 'fish out' piece A from the water, resulting in A–B turbostratic bilayer graphene on the copper foil. After overnight drying and an additional 200 °C, 10 min bake, the A–B bilayer graphene piece was placed into copper etchant again. After the second etching, it was transferred onto tattoo paper, as described above. It is important to note here that the resulting A–B stack of graphene is what we call the bilayer graphene; it is morphologically and electronically different from specifically CVD-grown A–B stacked bilayer graphene. 3L-GETs were fabricated in a similar manner, creating A–B–B stacked graphene layers.

The graphene transfer process was fast; it took less than 1 min to transfer an array of six (two injecting and four sensing) GETs (Supplementary Video 2). Two batches of six GETs were transferred onto each participant, one batch over the ulnar artery, one batch over the radial artery. The GETs were pre-designed and positioned with 8 mm pitch, allowing us to precisely control the spacing between GETs and reducing measurement variability.

Graphene–skin impedance measurements. Graphene–skin impedance was studied using the Hioki LCR meter IM3536, allowing a frequency sweep from 4 Hz up to 8 MHz. The frequency range used in this study, however, was narrowed down to 10 Hz–1 MHz. The measurements were performed in the constan-voltage mode and 50 mV a.c. amplitude with no d.c. bias. Each data point was measured four times and averaged. The frequency sweep was performed three consecutive times, each sweep taking approximately 90 s, with 10 s delay between sweeps.

Bio-Z measurement set-up. The variable part of the impedance, ΔZ_{artery}, typically minimal in amplitude (below or equal to 50 mΩ), represents the changes in blood volume in the artery, extracted by digital signal processing algorithms or high-quality detection of the arterial pulse signal. The low-noise multichannel Bio-Z sensing hardware, the so-called XL-board, was explicitly designed to capture the slight variations in Bio-Z with high resolution (Methods and Supplementary Figs. 21–23). A custom printed circuit board was designed to provide low-noise Bio-Z sensing for this study, as shown in Supplementary Fig. 21. The hardware was built around the ARM Cortex M4 microcontroller (MCU), which transfers the user-defined digital waveform to the a.c. current signal by passing a 16-bit digital-to-analogue converter (DAC, Texas Instruments). The MCU controls the frequency and amplitude of the current signal. In turn, the DAC generates an analogue signal used in a negative feedback loop on a low-noise operational amplifier (Texas Instruments) to generate an a.c. current signal with programmable amplitude and frequency (Supplementary Fig. 22). A series capacitor at the DAC output was used to circumvent the need for the injection of a d.c. current component into the human body. The signal from the impedance-sensing electrodes was filtered through a high-pass filter. To obtain the Bio-Z, we measured the voltage modulation associated with the injected current modulation. The signal was then amplified with a low-noise instrumentation amplifier. A high-precision analogue-to-digital converter facilitated the instrumentation amplifier output through an analogue anti-aliasing low-pass filter. The analogue-to-digital converter (Texas Instruments) sampled the voltage at a frequency of 93.75 kHz with 24-bit (0.3 μV) resolution to provide sufficient precision. The analogue front end and the MCU could simultaneously measure ten independent Bio-Z streams and various analogue readings. The analogue front end was powered up with a regulated ±5 V supply for digital and analogue operations. Injecting 1 mA with 5 V limit led to a suggested value of the maximum interface impedance of 5 kΩ, up to which no analogue front end saturation would occur. Above this impedance, we needed to decrease the injected a.c. current proportionally, decreasing the signal-to-noise ratio (SNR) proportionally of the measurements. Hence, current injecting electrodes of the lowest impedance are most suitable. In this study, the first four channels were selected for high-resolution Bio-Z sensing, and the fifth channel was reserved for simultaneous PPG readings used for syncing with the Finapres NOVA BP system. The sampled data were forwarded to a PC via the MCU and a high-speed USB bridge for signal post-processing. Supplementary Fig. 4a shows the block diagram of the multichannel Bio-Z measurement set-up. When recording Bio-Z signals, each participant wore additional sensors alongside the GETs: a BP brachial cuff and finger cuff (Finapres NOVA) and two PPG sensors. The two PPG sensors allowed us to precisely correlate the timing of the events between the XL-board and the Finapres device.

Experiments with human participants. The experiments with human participants were performed under the approval of the Institutional Review Board of the University of Texas A&M (IRB no. IRB2017-0335D). A total of $N=7$ participants in their mid-twenties participated in this proof-of-principle study. One participant performed GET experiments with a cycling-enabled BP elevation routine. Six participants performed GET experiments with HGCP-based BP elevation. One participant performed both GET and Ag wristband experiments for direct comparison. Five participants performed the Valsalva manoeuvre for BP elevation, a series of mild exercises and post-workout HGCP model validation experiments. Each experimental routine lasted at least 4 ± 1 h on average. One individual HGCP pattern took ~450 s of continuous data collection, and an average of 5 ± 1 HGCP manoeuvre patterns were performed by each participant, comprising a total of ~$2{,}500\pm600$ samples (beats) used for algorithm training and ~250 ± 60 samples used for algorithm testing (see Supplementary Tables 3–9 for details of each participant). The Valsalva routines comprised an average of 300 ± 150 samples, and cycling routines consisted of ~615 samples that were considered for model training and testing.

Common mode rejection and signal cleansing with ground connection. Bio-Z sensing is a highly noise-susceptible operation. An additional common ground (GND) connection was established with the skin to reject the common mode noise elements and provide a stable reference for the instrumentational amplifiers. The location of the GND electrode was chosen arbitrarily, typically on the same forearm (Supplementary Fig. 6). This extra electrode placement resulted in amplification in the detected Bio-Z signal. Hence, the pulsatile activity became more prominent, as shown in Supplementary Fig. 23 (ref. [37]).

Bio-Z signal processing. The signal acquired with the XL-board was bandpass filtered (second-order Butterworth) centred around the driving a.c. frequency to remove the residual d.c. offset, 60 Hz interference and high-frequency noise. Then, Bio-Z was extracted using simultaneous demodulation by multiplying the filtered signal by the injection signal generated by the MCU (Supplementary Fig. 4). The multiplier output was low-pass filtered (second-order Butterworth) with a cutoff frequency of 6 Hz to remove the carrier signal distortion and out-of-band noise while still allowing us to measure extreme maximum heart rates. The hardware was calibrated before the operation by measuring a known resistor's impedance to convert the measured voltage to an accurate resistance value. The measurement system can measure impedance with a root mean squared error of less than 1 mΩ, which is much lower compared than the target Bio-Z variations.

Signal abstraction, feature extraction and BP regression model. Four characteristic points abstracted the recorded $\Delta Z_{artery}(t)$ signals for each heartbeat. The ΔZ_{artery} peak corresponded to the DBP, whereas the most pronounced minima corresponded to the SBP. The second smaller peak and minima in the middle of the cardiac cycle corresponded to the back reflection of the pressure pulse. In addition to SBP and DBP, we leveraged the aforementioned characteristic points to estimate the MAP. We extracted the reference MAP from the BP waveform by taking the area under the BP curve normalized by cycle duration. To effectively detect DBP, SBP and MAP, we used four characteristic points from all phases of the cardiac pulse of the $\Delta Z_{artery}(t)$ signal: (1) diastolic peak, (2) maximum slope, (3) systolic foot (SYS) and (4) inflection point. The diastolic peak and SYS were estimated using the intersection of the tangent to the slope with the horizontal line from the maximum and the minimum of the signal, respectively. The maximum slope was estimated as the point in the middle of the descending slope section. The inflection point was the maximum slope point between the second peak and the notch. The points were identified from the first and the second derivative of the $\Delta Z_{artery}(t)$ signal using the zero crossing, peak and foot points.

PTT, the time it takes for the pulse to travel between two sensing sites on one artery, was selected as one of our main features of the BP. BP has an inverse quadratic relation with PTT. The ratio between the amplitudes of SYS and the inflection point relative to the diastolic peak is a measure of the reflection wave's intensity. The time interval between SYS and the inflection point measured the arterial stiffness, whereas the area under the curve represented the total peripheral resistance. All the features mentioned above were useful in modelling the arteries' cardiovascular properties, and we used them to build our regression model for BP estimation. The characteristic points of the $Z_{artery}(t)$ signals mentioned above were used to generate as many as 50 features for each heartbeat. The features were categorized into four sets, such as PTT, timepoint, amplitude and area. The PTT features were calculated from every possible pair of signals; other elements were computed from each signal individually. To smooth the data and filter out the beat-to-beat variations, we used window-based averaging (20 adjacent beats with a 50% overlap).

For each model, the hyperparameters were selected by splitting the training data: 89% were used to estimate the model parameters, and the remaining 11% were used for performance evaluation. The hyperparameters of the AdaBoost model consist of the number of the decision trees and the tree depth, which were selected from 8 or 16 for the number of trees and 4 or 8 for the tree depth that achieved the lowest error in the validation dataset.

The DBP, SBP and MAP were finally estimated using an advanced regression model trained by the $\Delta Z_{artery}(t)$ features extracted and BP data measured simultaneously by a reference continuous BP monitoring device (Finapres, NOVA). Our method provided brachial BP values from the wrist pulse signals' features as the regression training model used brachial BP data. To effectively estimate the BP, we needed to measure multiple values of both DBP and SBP during the training cycle. Therefore, such a training cycle usually consists of a series of exercises followed by a short relaxation state. Our participant-specific models (separate for SBP and DBP) were trained using a minimal number of training window samples for each participant, requiring careful model selection to avoid overfitting. We used the AdaBoost regression model based on ensemble learning that builds the prediction by combining several weak learners' outputs through a weighted sum of different subsets of the training dataset. The BP estimation performance was evaluated through training and testing the BP models on different subsets of the data as follows. First, The HGCP data for each participant were shuffled and then divided into ten folds to apply cross-validation by training the model using 9 folds (90% of the data) and testing the model on the remaining fold (10% of the data) ten times by changing the testing fold each time to cover the whole data and avoid the bias for training the model with a certain part of the data (Supplementary Fig. 16). Once the training cycle and regression model were complete, we used the regression model to directly output the BP(t) from the measured $\Delta Z_{artery}(t)$. The performance of the models was evaluated using the average across all the ten folds of the BP's root mean squared error. Second, the HGCP and Valsalva manoeuvre data for each participant were used for model training based on tenfold cross-validation, similar to the previous case but without shuffling to test capability of the the model to estimate BP for a continuous time segment. Third, each participant's Valsalva data were the only data used for model training based on tenfold cross-validation without shuffling to measure the capability to train the model with a small amount of data. Fourth, the HGCP and Valsalva data only were used to train a single model for each participant, which was tested on the post-workout data to evaluate the BP estimation in the future and after a workout. Finally, for participant 1, a model was trained by the HGCP and Valsalva data that were collected on the first day, then the model was tested on HGCP data measured after 4 days to evaluate the repeatability of BP estimation after multiple days.

Respiration rate extraction. A digital sixth-order Butterworth bandpass filter was applied to the $\Delta Z_{artery}(t)$ signal with cutoffs at 0.05 to 0.5 Hz. The resultant signal contained the baseband information that is modulated by the respiration rate. To capture the continuous rate information from the baseband signal, the signal was segmented into 2 min windows. Fast Fourier transformation was applied for each segment, and the dominant frequency component was picked using peak detection in the plausible range of 0.1 to 0.5 Hz. This value was selected as the respiration rate in hertz and multiplied by 60 to obtain a respiration rate in breaths-per-minute. The algorithms used to acquire the respiration rate were implemented in MATLAB R2019b.

Ethics statement. The human participant BP measurements were performed under the approval of the Institutional Review Board of the Texas A&M University (IRB no. IRB2017-0335D). The tattoo characterization experiments were performed under the approval of the Institutional Review Board of the University of Texas at Austin (IRB no. 2018-06-0058).

Reporting summary. Further information on research design is available in the Nature Research Reporting Summary linked to this article.

Data availability

The complete dataset supporting the findings of this study is available via the PhysioNet data repository at https://doi.org/10.13026/qcc8-n557. The associated preprocessed raw data are available and can be shared with interested parties upon reasonable request. Source data are provided with this paper.

Code availability

The machine learning algorithm is publicly available via GitHub at https://github.com/TAMU-ESP/Graphene_BP. The custom codes used for data visualization are available from the corresponding authors upon request.

Acknowledgements

The work was supported in part by the Office of Naval Research under grant number N00014-18-1-2706, the Temple Foundation Endowed Professorship, the National Science Foundation under grant number 1738293 and the National Institute of Health under grant number 1R01EB028106. R.J. acknowledges useful discussions with the former founding director of the National Institute of Biomedical Imaging and Bioengineering (NIBIB) at the NIH, R. I. Pettigrew. We acknowledge J. Wozniak at the Texas Advanced Computing Center (TACC) at The University of Texas at Austin (http://www.tacc.utexas.edu) for creating Fig. 1a. The authors have permission to use and publish the image.

Author contributions

D.K., K.S., R.J. and D.A. conceived the idea of using GET and designed the experiments. B.I. and R.J. designed the instrumentation for bioimpedance acquisition. D.K. fabricated and characterized the GETs. K.S. and B.I. optimized the XL-board. D.K., K.S., B.I. and N.K. performed the BP experiments. B.I. and A.A. developed and utilized the machine learning algorithm. D.K. and K.S. compiled and analysed the data. The manuscript was written with the contributions of all authors. All authors have approved the final version of the manuscript.

Competing interests

R.J. and B.I. filed a patent (US 2020/0138303 titled 'System and method for cuff-less blood pressure monitoring') related to this research; this patent is licensed to SpectroBeat LLC.

Additional information

Supplementary information The online version contains supplementary material available at https://doi.org/10.1038/s41565-022-01145-w.

Correspondence and requests for materials should be addressed to Roozbeh Jafari or Deji Akinwande.

Peer review information *Nature Nanotechnology* thanks Yingying Zhang and the other, anonymous, reviewer(s) for their contribution to the peer review of this work.

nature research

Corresponding author(s): Deji Akinwande, Roozbeh Jafari

Last updated by author(s): Mar 29, 2022

Reporting Summary

Nature Research wishes to improve the reproducibility of the work that we publish. This form provides structure for consistency and transparency in reporting. For further information on Nature Research policies, see our Editorial Policies and the Editorial Policy Checklist.

Statistics

For all statistical analyses, confirm that the following items are present in the figure legend, table legend, main text, or Methods section.

n/a	Confirmed	
☐	☒	The exact sample size (*n*) for each experimental group/condition, given as a discrete number and unit of measurement
☐	☒	A statement on whether measurements were taken from distinct samples or whether the same sample was measured repeatedly
☒	☐	The statistical test(s) used AND whether they are one- or two-sided *Only common tests should be described solely by name; describe more complex techniques in the Methods section.*
☒	☐	A description of all covariates tested
☒	☐	A description of any assumptions or corrections, such as tests of normality and adjustment for multiple comparisons
☐	☒	A full description of the statistical parameters including central tendency (e.g. means) or other basic estimates (e.g. regression coefficient) AND variation (e.g. standard deviation) or associated estimates of uncertainty (e.g. confidence intervals)
☒	☐	For null hypothesis testing, the test statistic (e.g. *F*, *t*, *r*) with confidence intervals, effect sizes, degrees of freedom and *P* value noted *Give P values as exact values whenever suitable.*
☒	☐	For Bayesian analysis, information on the choice of priors and Markov chain Monte Carlo settings
☐	☒	For hierarchical and complex designs, identification of the appropriate level for tests and full reporting of outcomes
☐	☒	Estimates of effect sizes (e.g. Cohen's *d*, Pearson's *r*), indicating how they were calculated

Our web collection on statistics for biologists contains articles on many of the points above.

Software and code

Policy information about availability of computer code

Data collection	Hioki LCR Sample Application; Hioki HiTESTER; Keysight GUI Data Logger Software For Handheld LCR Meter; Finapres® NOVA, Visual Studio
Data analysis	MS Excel, Origin Pro, MATLAB, Python 3

For manuscripts utilizing custom algorithms or software that are central to the research but not yet described in published literature, software must be made available to editors and reviewers. We strongly encourage code deposition in a community repository (e.g. GitHub). See the Nature Research guidelines for submitting code & software for further information.

Data

Policy information about availability of data

All manuscripts must include a data availability statement. This statement should provide the following information, where applicable:

- Accession codes, unique identifiers, or web links for publicly available datasets
- A list of figures that have associated raw data
- A description of any restrictions on data availability

The complete dataset supporting the findings of this study is available in PhysioNet data repository. The associated pre-processed raw data is available and can be shared with interested parties upon reasonable request.

Field-specific reporting

Please select the one below that is the best fit for your research. If you are not sure, read the appropriate sections before making your selection.

☒ Life sciences ☐ Behavioural & social sciences ☐ Ecological, evolutionary & environmental sciences

For a reference copy of the document with all sections, see nature.com/documents/nr-reporting-summary-flat.pdf

Life sciences study design

All studies must disclose on these points even when the disclosure is negative.

Sample size	N=7 subjects have participated in the study. N=6 of the participants have performed HGCP experimental routine, which consists of at least 5, up to 7 repetitive sets of measurements. Each measurement set is split into 4-5 iterations, approximately 90 seconds each. The calibration Finapres Nova was running interchangeably, with measurements stopped every 15-20 minutes because of the pressure applied onto subject's finger, and time was given for subjects to ease up. N=5 subjects performed Valsalva maneuver and N=1 subject performed cycling exercise. During impedance measurements, at least three tattoos of each kind were were used as a single set, recording three pairs: 1-2, 1-3, and 2-3. Each time the sweep was performed three times with 10 sec interval.
Data exclusions	Occasionally, the extensive pressure applied by the finapres NOVA's finger cuff, and possible misplacement of the reader, have resulted in conditionally wrong collection of "training/true" data. When at rest conditions we saw the DBP values above 140 and SBP values above 160, those trials were excluded from the evaluation.
Replication	Each subject's BP and Bio-Z was measured at minimum 5 times, each with 4-5 iterations, approximately 90 seconds each. Two sets of each graphene type (multuple GETs per type) were used to perform graphene tattoo characterization study.
Randomization	Not applicable.
Blinding	Not applicable.

Reporting for specific materials, systems and methods

We require information from authors about some types of materials, experimental systems and methods used in many studies. Here, indicate whether each material, system or method listed is relevant to your study. If you are not sure if a list item applies to your research, read the appropriate section before selecting a response.

Materials & experimental systems

n/a	Involved in the study
☒	☐ Antibodies
☒	☐ Eukaryotic cell lines
☒	☐ Palaeontology and archaeology
☒	☐ Animals and other organisms
☐	☒ Human research participants
☒	☐ Clinical data
☒	☐ Dual use research of concern

Methods

n/a	Involved in the study
☒	☐ ChIP-seq
☒	☐ Flow cytometry
☒	☐ MRI-based neuroimaging

Human research participants

Policy information about studies involving human research participants

Population characteristics	Total N=7 presumably healthy subjects (age 18-35) participated in the study, N=6 male and N=1 female.
Recruitment	The recruitment was performed in full accordance to the IRB protocol.
Ethics oversight	Institutional Review Board of the Texas A&M University (IRB no. IRB2017-0335D) Institutional Review Board of the University of Texas at Austin (IRB no. 2018-06-0058)

Note that full information on the approval of the study protocol must also be provided in the manuscript.